

## A LES STUDY OF TURBULENT FLOW AROUND TWISTED AND TAPERED CANTILEVER.

J. Lorentzon<sup>1</sup>, J. Revstedt<sup>2</sup>

<sup>1</sup> PhD Student, Department of Theoretical Chemistry, Lund University, P.O. Box 124, 221 00  
Lund, Sweden, johan.lorentzon@teokem.lu.se

<sup>2</sup> Professor, Department of Energy Sciences, LTH, Lunds University, P.O. Box 118, 221 00  
Lund, Sweden, johan.revstedt@energy.lth.se

**Key words:** *LES, DMD, VIV*

A study was performed on the passive control of Vortex-Induced Vibrations (VIV) for three different geometric forms of cantilever twisted/taper/taper-twisted subjected to a turbulent flow. The method used is LES with dynamic Smagorinsky model, TVD spatial scheme and backward difference scheme in time. The results show a reduction of the drag coefficient ( $C_d$ ) on mean by 5% and a reduction of the RMS of lift coefficient ( $C_l$ ) by 50/80% for taper/twisted configuration, which is consistent with related studies. DMD analysis also show that the shear layer around the cantilever is desynchronized but further downstream it re-synchronize prior to the re-attachment point of the flow. This lead to a larger wake and street vortex with shape that reflects the deformation of the cantilever.

### Introduction

The understanding of how a fluid interacts with a bluff body is an important subject, with many applications in engineering such as architecture, airfoils, turbines or vehicles. The main phenomena of interest is to study the separation of the flow over the sides of the body which due to the induced shear at surface and the forced deflection around the body, redistributes the motion of shear flow into vortices. As a result, a mixing layer appears around the body with recirculation zones on the sides tranverse to the flow and on the lee side the layers oscillates and forms downstream a trail of vortices. These vortices are for sufficient large aspect ratio (AR) with respect to height released in a periodic asymmetric manner, known as vortex shedding, a characteristic difference between a streamlined body and a bluff body. The flow is characterized by the Reynolds number ( $Re = \frac{UD}{\mu}$ , where  $\mu$  is the kinematic viscosity,  $D$  the characteristic length and  $U$  the mean velocity). However, the frequency  $f$  of vortex shedding, expressed in a non-dimensional units, Strouhals number ( $St = \frac{Df}{U}$ ), vary only weakly with  $Re$  with a value around 0.1-0.2. The force oscillations caused by the vortex shedding induces vibrations in the body. The

strength and frequency may be calculated from lift and drag coefficients which in turn can be deduced from the pressure distribution on the cantilever surface by neglecting skin friction. In understanding this interaction lies the ability to control the forces induced by the surface shape of the body such that it maximize/minimize force fluctuations depending on the application. Several studies reports on cases with rectangular prism with different design parameters. The most commonly used is the aspect ratio (AR) of cross-section and height. Another parameter is the orientation with respect to the main flow direction (inclination angle). The corner/edge effect is another important factor, a sphere interacts differently than a cube and similar the flow directional onto a flat surface interacts different compared to the flow upon a edge/corner. Twisting the cantilever by rotating the cross-section as a function of height is of interest to remove the dependency of flow direction, whenever circular cross section is not feasible. In a review on the subject of aerodynamic modification on buildings [1] there is no known studies on shape by twisting with free-end twisted cantilever. Only two CFD studies prior 2014 has been found since 2010 [2, 3] and both articles uses instant pictures and mean value properties to describe the flow which is insufficient to described the wake dynamics satisfactory. Giving a detailed quantitative description of the wake structure is a challenge. Often used in this context is statistical properties such as contour plots of mean fields and root mean square (RMS) over the domain, or at probe points autocorrelation matrix (R), Fast Fourier Transform (FFT) spectra and power spectra (PSD) for the velocity components. In addition, coherent patterns can be visualized by the eigenvectors of the R matrix, using Proper Orthogonal Decomposition (POD), which captures the motion, however in mixed frequencies. A recently developed technique [4], the Dynamic Mode Decomposition (DMD), suitable to study stationary processes, has been succesfully applied to wake structures of cylinders [5]. In DMD, one obtains frequency and modes shapes of coherent structures. When applied to velocity fields this provides a measure of the strength of vortices and the duration time. The aim for this study is to use the DMD to investigate the difference between the regular (i.e. a constant quadratic cross-section) and different design of cantilever and thus complement the available studies with a more detailed description of the dynamics of the wake.

## Method and Numerical Details

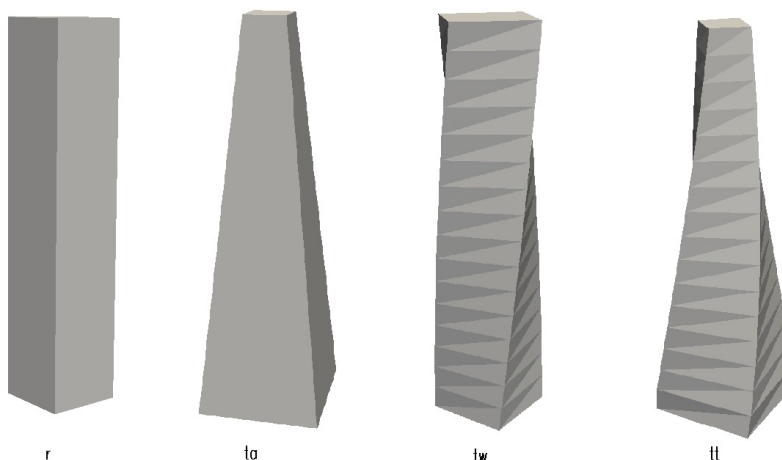
The incompressible Navier-Stokes equations (NS) are solved by pisoFoam from the OpenFoam package[6], which uses the Finite Volume Method (FVM) implemented as a segregated solver using the PISO algorithm. The OpenFoam implements the Gauss finite volume integration approach where one evaluates integrals by summation of the face values obtained by interpolation from cell center values. The schemes has to be specified for the temporal, divergence, laplacian and gradients term in the (NS) equation. In the present study, as temporal discretization, the backward scheme is used and for the divergence scheme the TVD [7] scheme was chosen with the limiter scalar parameter set to 0.1, where 0 is for most accurate and 1 for most stable. For the laplacian and gradient terms, a central difference scheme (CD) is chosen. To ensure boundness for gradients, a cell limiter is applied and for unstructured mesh the lapacian scheme is corrected for

the non-orthogonality. LES is used as turbulence model with the homogenous dynamic Smagorinsky as subgrid scale model (SGS) [8]. The chosen schemes are taken from a pre-study where several different schemes were compared, guided by a related study [9]: from the PSD, the criteria in choosing model were the largest obtained proportion of the inertial range down to the cut-off defined by the mesh. The Taylor length scale is estimated to 0.8 mm by Kolmogorov length scale (0.2 mm) and relative scale ( $\sim 4$ ). From this study the least dissipative scheme with explicit SGS is the optimal choice but as long the mesh were sufficient fine (cell size  $< D/20$ ) the choice of SGS is less significant than compared to discretization scheme. The implicit-LES with the linear upwind scheme (ILES) [10] gave an initial range that started later with a too steep slope and sensitive to mesh structure. Another model studied, the local dynamic Smagorinsky with no backscatter had improper shape of PSD.

## Domain description and Mesh generation

The fluid is velocity driven with an uniform flow across the inlet of 1 m/s, no-slip condition at the floor and the cantilever and slip condition is used for the other walls. The pressure is set to zero-gauge pressure at outlet. A cantilever with dimension  $(5 \times 1 \times 1)D^3$  [ $D=0.2$  m] is placed in a rectangular domain  $(31 \times 16 \times 12.5)D^3$  with 10D from inlet, 20D from outlet and 7.5D from the walls. The Reynold number is 5000 with respect to D and inlet velocity. The mesh is unstructured and generated by using Gmsh [11] (tetrahedrons). It's refined in the wake until convergence with respect to the RMS of the velocity field (threshold 0.01 m/s) yielding a total 5 MCell mesh. The blockage ratio is 2.5% and the effect of this in shedding is neglected, the Maskell correction. Turbulence in the inlet would reduce the drag, lift and suction pressure and should be considered while comparing to experiments but also these effects are neglected. Further discussion on blockage correction and experimental considerations can be found in the work by Sohankar et al [10]. The mesh on finest scale is of factor 10 larger from Taylor length scale, in a pre-study on a refined mesh on regular case, gave no further improvement apart the high gradient regions, the border of the wake and the entrainment around the cantilever. The probes are placed regularly around the cantilever and downstream ( $> 50$  points). In this study, three modified cantilever designs are considered in order to disrupt the wake mechanism: tapering for which the vortex shedding frequency varies over the cantilever height, twisting which causes desynchronizaton of the shear layers on either side of the cantilever, and a combined case which is a combination of both, see Figure 1. The design of the cantilevers is such that for 2D plane cut throught the midsection of the cantilever has the same geometric profile for all cases and *equal* frontal area. In the following, the flow direction is in the X direction, axial direction of cantilever the Z direction. The Y axis is refered as the transverse direction to the flow direction.

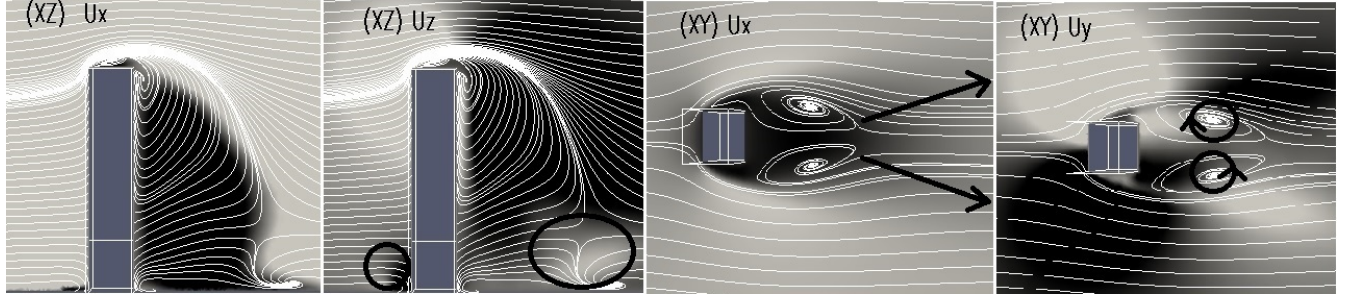
Figure 1: Geometric shape of the cantilever considered: regular (r), taper (ta), twisted (tw) and combined (tt)



## DMD

The proper orthogonal method (POD) is a tool for studying coherent motion, using the eigenvectors of the autocorrelation matrix for a given sequence of data over time. The disadvantage of this method is that it contains multifrequency processes that one would want to visualize separately. The Dynamical Mode Decomposition (DMD), is similar to Discrete Fourier Transform and used for the purpose to extract coherent pattern of a certain frequency obtained from probe analysis. For a sufficiently large collection of measurement of a variable such as the velocity field, the DMD representation is exact and in comparison to POD which captures larger structures the DMD has the ability to describe finer motion of stationary character. From the DMD analysis one obtains to each mode a weight based upon the norm used ( in this article the L1 norm is applied) and each mode is characterized by the decay coefficient and oscillation frequency. A measurement is the field for given time. The assumption is that for each subsequent field is related by a Koopman operator operating on the present field [4]. Thus all observations can be generated by successive multiplication of this operator from a starting field. The error in this approximation is collected in the last observation field, hence when the number of observations equals the dimension of the field, this representation becomes exact. When applied to velocity field, the autocorrelation is proportional to the kinetic energy and is a measure of the energetic content in a flow.

Figure 2: Streamline plot of the regular case in (XZ) plane ( $Y=0$ ) and (XY) plane ( $X=11.5D$ ), the sign of components indicated by white/black (+/-), from left to right: (1)  $U_x$ , (2)  $U_z$ , (3)  $U_x$ , (4)  $U_y$ . (1) illustrates the areas of reverse flow, the wake and necklace, (2) note the upward flow on lee side, the upwash at (RP) (3) shows the reverse flow in wake and the direction of vortices in the Karman vortex street, (4) illustrates the recirculation of of opposite sign in the wake

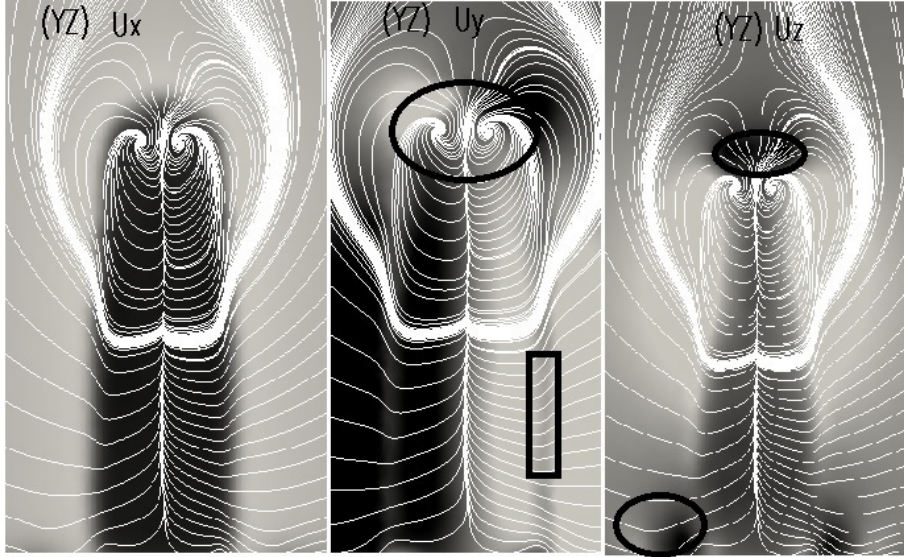


## Simulations and Results

### The wake mechanism in detail for the regular case

The approaching flow from the inlet is divided at the stagnation point (SP) on the frontside of the cantilever into an upward and a downward going flow ( $Z$ ), as expected for cantilevers above the critical aspect ratio (height/ $D$ ) [14]. A necklace (horse-shoe) of base vortices is formed at the base of the cantilever. The boundary layer is around  $0.5D$  at the front of the cantilever. The flow around the cantilever body is separated into a pair of oscillating shear layers in tranverse direction ( $Y$ ) with a recirculation zone *without* span-wise oscillation nodes along axial direction of cantilever ( $Z$ ). The upgoing flow is separated at the free-end with no re-attachement and the entrainment on the cross-section side (XZ), starting from the (SP) is going upwards, is synchronized with the free-end side vortices that oscillates in stream-wise direction. Two recirculation zones are observed on the free-end surface. By studying the flow from starting time to the point when the flow is fully developed, the recirculation from the tranverse sides to the cantilever is expanding downstream, leading to an elongated tail that starts to oscillate (synchronization). When the opposite recirculation zones on each side of the cantilever couples and oscillates, it forms pairs of counter rotating vortices which at re-attachement point (RP) splits into two expanding vortices whose motion upwards is much like a tromb while the downwash cuts down the wake by mixing from the topside. The release of vortices, i.e. vortex-shedding, induces a beating on the cantilever which can be detected in the lift coefficient data. Beyond the (RP) span-wise oriented vortices are transported to the outlet in a zig-zag formation, the von Karman vortex street. In the free shear layer around the body one can observe the Kelvin-Helmoltz instability (K-H) in (YZ) plane as a thin section in mean velocity plot between inside the wake and outside with near zero field (oscillation). The results matches those obtained both experimentally and from simulations for closely related studies [12, 15]. Below the critical AR the downward flow is absent, and the flow then becomes different with symmetric release of vortices known as arch-type vortex street [14, 16]

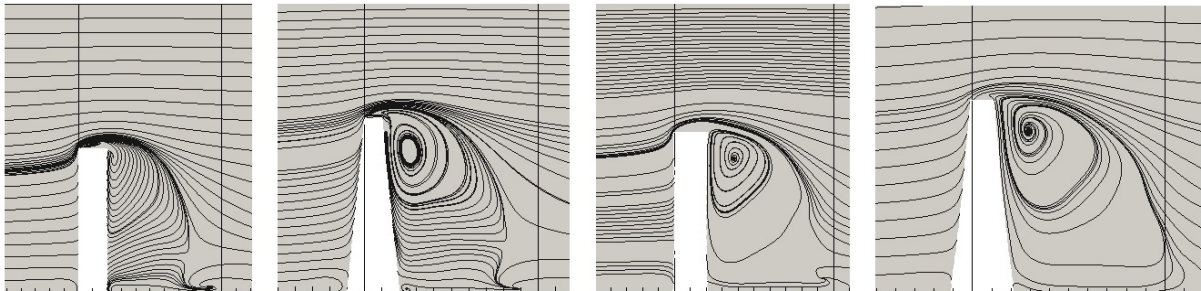
Figure 3: Streamline plot of regular case in (YZ) plane ( $X=11.5D$ ) on lee side of the cantilever, the sign of components indicated by white/black (+/-), from left to right: (1)  $U_x$ , (2)  $U_y$ , (3)  $U_z$ . (1) illustrates the areas of reverse flow, the wake and necklace (weak), (2) shows the in rectangular area the region where (K-H) is located (rectangular box), the downwash vortices from the tip (3) shows the downward directed flow and the horse-hoe vorticies



### Mean field properties of velocity

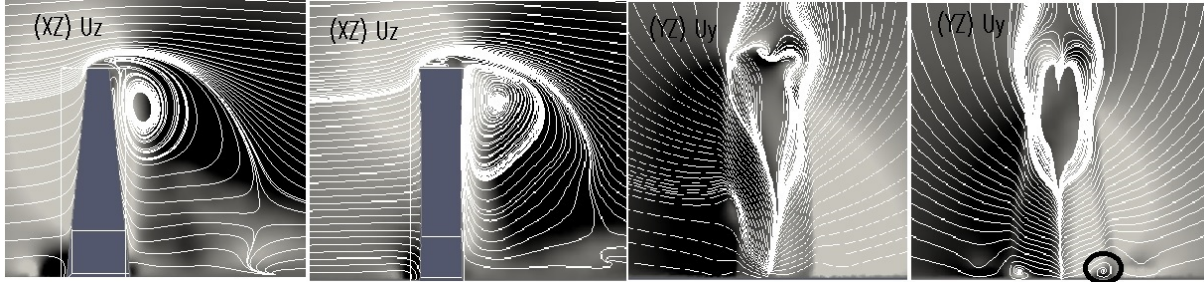
The streamline plot of the mean field for all four cases is similar from the mid section cut plane, see Figure 4. However, by coloring the background of the plot with velocity components, a complementary description is obtained, see Figure 5 for a cutplane for  $tw$  and  $ta$  case, which shows the streamline plot of a cross-section ( $XZ$ ) at  $Y=0$  and cross-section ( $YZ$ ) at  $X=11.5D$ . From comparison of Figure 2 and 3 with Figure 5: The regular case has a stronger downwash, taper stronger upwash and the wake is not synchronized spanwise for twisted. The epicenter of the recirculation (ER) zone on the lee side of the tip is moved downstream by order of  $1D$  for all the designed cantilevers with respect to the regular case leading to stronger upward flow on lee side, not to be confused with entrainment. The re-attachement point is further downstream in the following order: *combined* > *twisting* > *taper* and also the upwash is stronger compared to the regular case. The wake size is increased for deformed cases in the following order: *taper* < *twisted*

Figure 4: Streamline of the mean velocity  $\bar{u}$  for ( $XZ$ ) plane ( $Y=0$ ) left to right:  $r$ ,  $ta$ ,  $tw$  and  $tt$ .



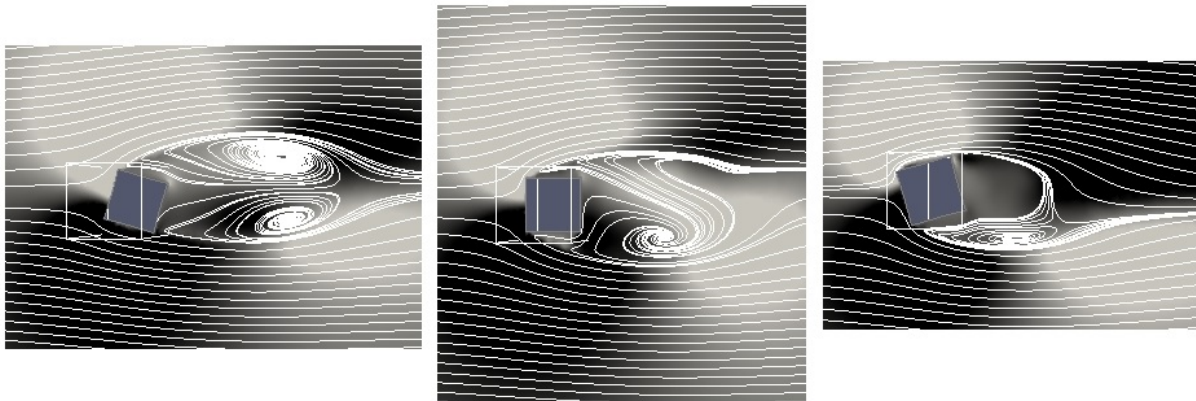
< *combined* which is consistent with the movement of the (ER) and (RP). In a study of

Figure 5: Streamline plot of *ta* and *tw* case in (YZ) plane ( $X=11.5D$ ) on lee side of the cantilever and cross-section (XZ) plane ( $Y=0$ ), the sign of components indicated by white/black (+/-), from left to right: (1)  $U_z$ , (2)  $U_z$ , (3)  $U_y$ , (4)  $U_y$ . (1) *ta*: larger diameter at base leads to larger horse-shoe and larger upwash and upper recirculation epicenter moved (2) *tw*: upper recirculation epicenter moved 1D (3) distorted tip alters the trailing vorticities and thus reduces the downwash that shapes the wake downward and thus increases the wake (4) slight reduced downwash and smaller recirculation zone leading to smaller downwash, note the inward going horse-hoe at base



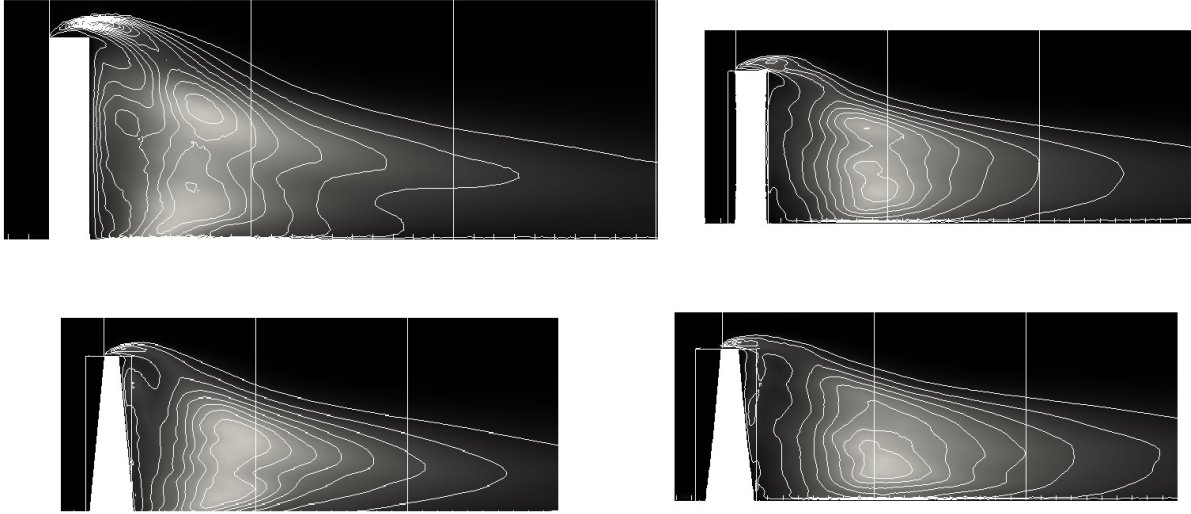
angle of inclination of a squared-prism cantilever [13], the streamline plot in cross-section (XY) is similar to the cut plane at height of corresponding angle in twisted form (*tw*). The recirculation zones differs significantly over height for twisted (Figure 6) and implicates no synchronization over the sides. The ordering of cases with respect of the maximum of

Figure 6: Streamline plot for *tw* case in (XY) plane at on lee side of the cantilever and cross-section (XZ), the sign of  $U_y$  components indicated by white/black (+/-), from left to right: (1) at base two elongated recirculations, (2) one recirculation zone (3) two recirculation zones



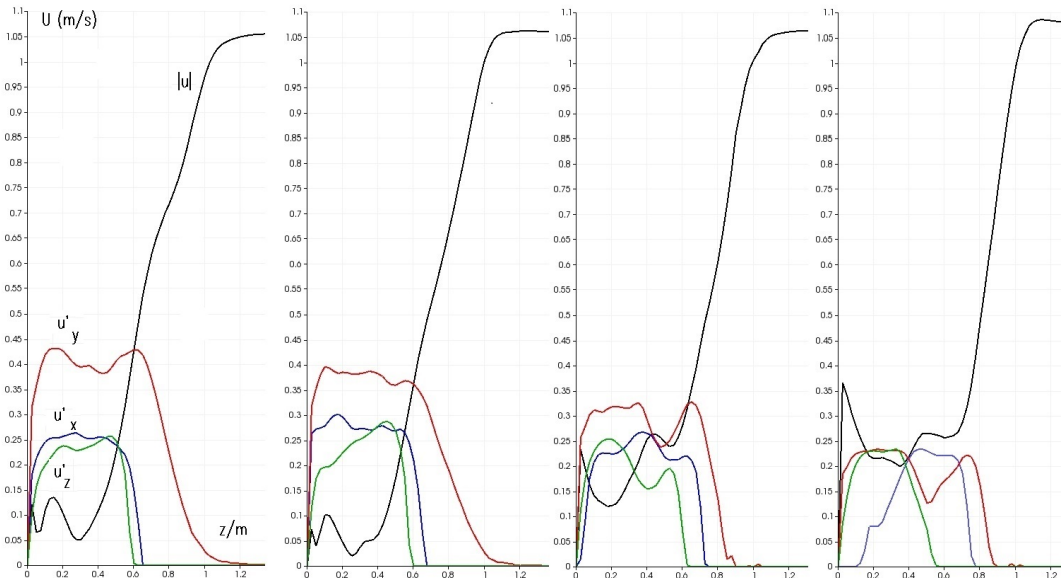
mean velocity [located at the shear layers around the cantilever due to (K-H)]: *combined* > *regular* > *taper* > *twisted*. Further, there is no significant difference between taper and regular in the wake structure indicating similar flow patterns, although different quantitatively such strength of vortices and their frequencies. The twisted forms (*tw+tt*) do, however, show significant differences with a lack of downwash mechanism and different structure of the recirculation zone compared to regular case. The dynamical content in the velocity is can also be illustrated by the RMS of the velocity fluctuations, see Figure 7. The ordering of cases with respect to the maximal RMS of velocity [located at the re-

Figure 7: RMS of  $u$ :  $r$  (large),  $ta$  ( $\downarrow$ ),  $tw$  ( $\rightarrow$ ) and  $tt$  ( $\searrow$ )



attachement point of the wake]: *regular* > *taper* > *twisted* > *combined*. In comparison to the work by Jung and Yoon [3], although applied to a case with circular cross-section and no free-end (period boundary), the differences between regular and twisting are, in our study, similar with respect reduction of RMS and the prediction for the location of maxima further downstream [3]. The contour of RMS in Figure 7 matches with the streamlines of the mean velocity for the two recirculation zones from Figure 4 and the estimated (RP) is in the region where the maxima of RMS for  $\bar{u}$  occurs (3D-5D). Figure 8 show the plot over line of the RSME for  $\bar{u}$  along the Z direction for 0-6D range at 4D from the edge of cantilever at midsection. At the re-attachement point the RMS appears as a broad band

Figure 8: Average velocity and RMS of velocity fluctuations along the cantilever height at 4D downstream of the cantilever edge for (from left to right) regular, tapered, twisted and combined case.



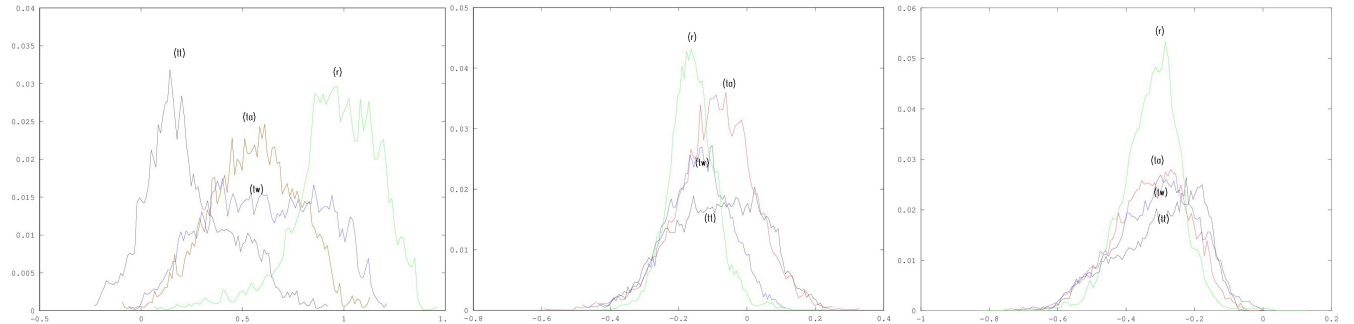
for all cases. If the plot were moved closer to the cantilever, differentiation will occurs

that reflects the difference in the geometries of the body. Wherever RMS of velocity peaks minima the mean value is peaks maximais consequence of the uniform inlet and that the pressure drops quickly after (RP). This is due to the *transfer* of kinetic energy from shear flow into vortices. Noteworthy is to observe the similarity between regular and taper case. The drop in x and z components of velocity fluctuations for regular and taper is due to the placement line is near of the edge and outside the flow is laminar due to uniform inlet.

### Probe analysis near cantilever

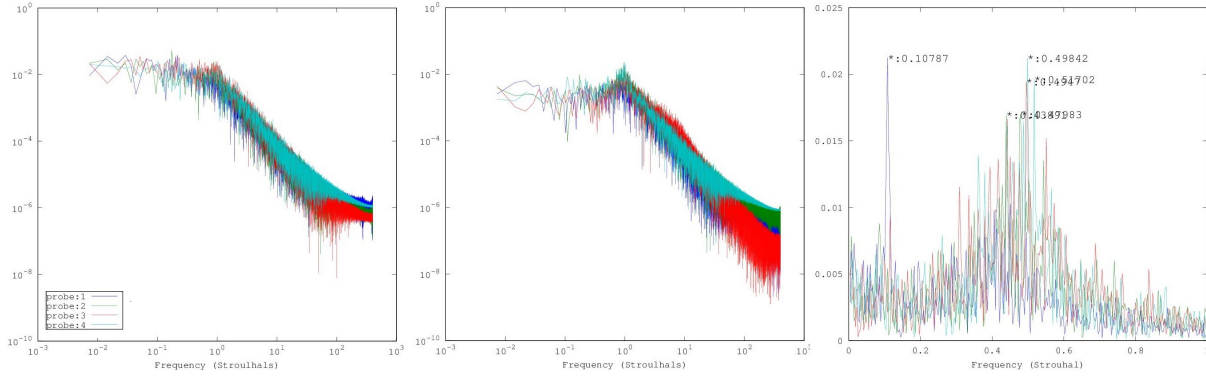
The distribution of rawdata of the velocity components  $U_x$ ,  $U_y$  and pressure at a probe point (11D,-1D,2.5D) is presented as histograms in Figure 9. At this location the recirculation of the flow attached to the cantilever is strong and marks beginning of vortex shedding. The pressure distribution is narrower for the regular and most wide for the twisted. Similar observation can be drawn for the distribution for velocity in transverse direction (Y) to the flow. The corresponding distribution of the velocity component in the flow direction (X) shows that the regular case has a more narrow, essentially centered around 1 m/s, while twisted and tapered both exhibit wider distributions centered around 0.5. The combined case has the lowest peak velocity and also shows a significant amount of back flow at this position. Although this is data from a single point only it gives an

Figure 9: Data distribution of (from left to right) velocity in the x-direction, velocity in the y-direction and the pressure. at (11D,-1D,2.5D): r(g) ta (r) tw (b) tt(black)



indication of the strong influence of the cantilever shape on the wake development. As is shown in Figure 10 below, the twisted case has larger energy in the inertial subrange of PSD (unfiltered) for velocity in Y (red) and regular the lowest (blue), this difference is more likely due to the transfer between velocity components due to the redirected flow over different cantilevers which is also reflected in Figure 9. The FFT of the pressure show both the shedding frequency (0.11 St) and the shear instability, the Kelvin-Helmholtz (K-H) frequency ( $\sim 0.5$  St), see Figure 10. These frequencies are masked in the integral log range for PSD spectra. The absence of sheddings frequency for twisting/combined implicates no synchronization in the shear layers. All cases shows a broad band of (K-H) and most plausible explanation is the slow oscillation in shear layer that is related to the intermittence of downwash.

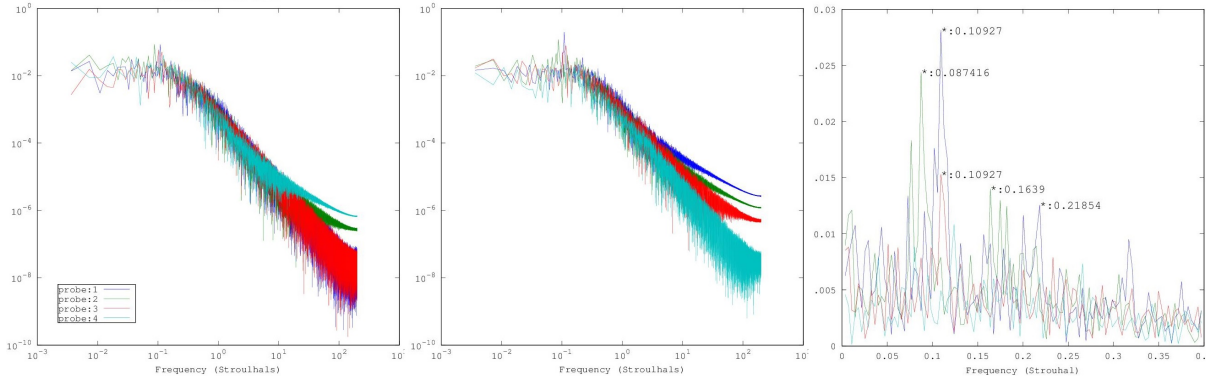
Figure 10: The PSD and FFT in following order: (left to right): PSD of  $U_x$ , PSD of  $U_y$ , FFT of pressure at (11D,-1D,2.5D): ), labeling according r(1) ta (2) tw (3) tt(4)



### Probe analysis in the vortex street

A probe analysis at a location downstream near the re-attachement point (16D,-1D, 2.5D), see Figure 11, for the pressure fluctuation, shows for the twisted case, a shedding frequency with same value as for the regular case, although with lower intensity. Further one finds an multiple frequencies for the shedding frequency for the regular and tapered case while it is not present for all other cases. The higher frequencies for the regular case are overtones to the lowest frequency. The difference in cutoff frequency (i.e. the highest frequency

Figure 11: The PSD and FFT in following order: (left to right): PSD of  $U_x$ , PSD of  $U_y$ , FFT of pressure at (16D,-1D,2.5D): ), labeling according r(1) ta (2) tw (3) tt(4)

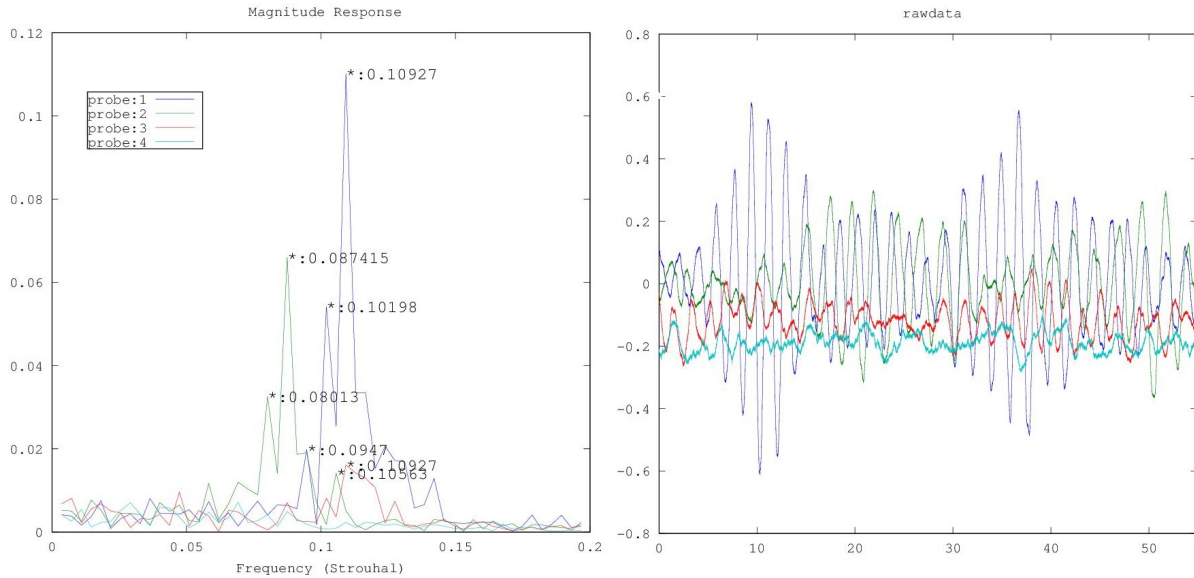


that can be resolved, which is determined by the grid resolution and the local convective velocity) can be related to the relative position of the probe to the (RP), the further from the point the smaller cutoff, see Figure 11. The intensity for the shedding frequency is larger and thus it is observed on both PSD and FFT spectra.

## Force statistics over the cantilever

The mean drag coefficient ( $C_d$ ) drops by 5% and RMS of the lift coefficient ( $C_l$ ) goes from regular case 0.18 to 0.04/0.03 for twisted/combined. For the twisted cases, the dynamics of the integrated force constants differst compared the regular case such that the  $C_l$  varies in time around a non-zero value (the offset). The results are consistent with previous studies [2, 3], where despite the difference in cross-sectional shape (circular) the same trend is observed regarding the changes in RMS for the twisted of  $C_l$  and the mean value of  $C_d$ . However the net force experienced is on average not reduced since the RMS of  $C_l$  for the regular is the same as the offset plus the RMS. This implicates that whenever one reduces the RMS, the larger becomes the offset, a conclusion that needs to be verified. The reduction of integrated force constants can be viewed as an force direction effect since curved surface makes the normal to the surface to point in different a direction for twisted and that tapering alters the shedding frequency and thus lessen the synchronization between shear layers. The shedding frequency has an envelope whose frequency matches the intermittence with entrainment and the sheddings frequency is decreases as larger the envelope becomes. The effect of twisted is therefore reduced by lessen the downwash, i.e. less entrainment implies smaller dynamic response.

**Figure 12:**  $C_l$  data to right and FFT to left: (1) r, (2) ta, (3) tw (4) tt

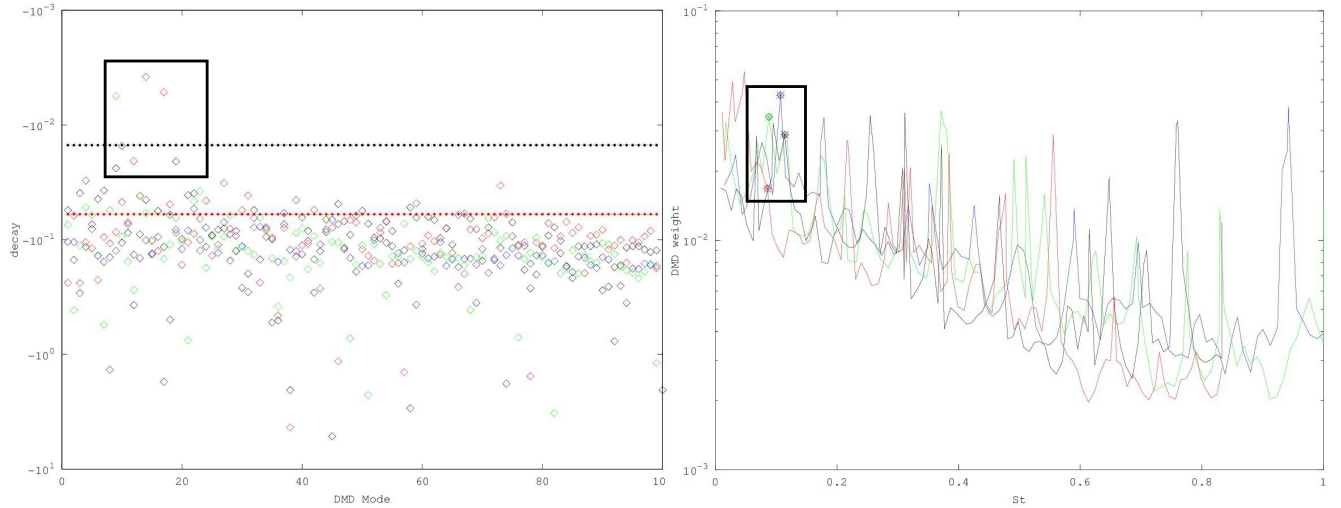


## DMD analysis

The rawdata of Figure 12 (right) is analyzed prior the DMD analysis. Using a sampling rate of 20 samples per period and sampling over than 10 periods provides an accuracy within 10 percent. It also allows to capture the Kelvin-Helmholtz frequency by four points per period, in total  $\sim 50$  periods sample. By construction, one DMD mode per

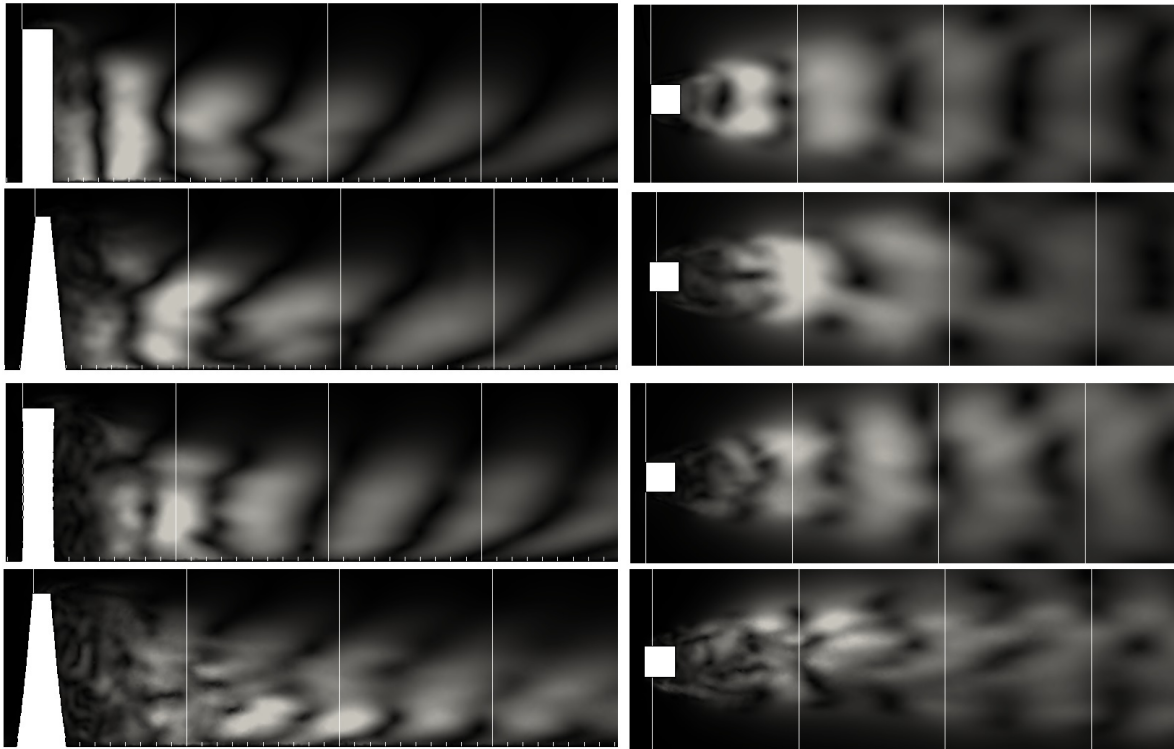
process was selected for study, see Figure 13. The selected DMD with frequencies and decay coefficients that matches with the shedding frequency where plotted, see Figure 14. To ensure proper selection, modes of nearby frequencies is studied but ruled out due to high decay coefficients corresponding to 1-2 periods of life time. Two flow mechanism

Figure 13: The DMD spectral analysis frequency plot (right) and lifetime of process (left), the nodes above the black line is DMD mode that is visible over the whole sampling time, below the red line the process is visible only 2 seconds or less. The four selected processes from figure right [boxed and marked] are within the box to the left



is captured by the DMD analysis, the (K-H) instability and the Karman vortex street. One significant outcome from the DMD analysis is that around the cantilever there is *no* synchronized motion for the deformed cases, but downstream the vortices synchronize prior (RP) point and the characteristic vortex shedding reappears after (RP), which is consistent with the differences in probe analysis in the previous sections and the lift coefficient data. The geometric form is reflected in the shape of the downstream shedding, for regular the sign of the DMD function is symmetric over the midline (hence nodal line is perpendicular to the flow), for twisted the sign is asymmetric over the midsection (with same frequency as for the regular), the taper is symmetric over midsection but with larger distance between nodal lines (lower frequency). The DMD frequencies with consideration taken for the slight increase in error in sampling, are consistent compared to probe analysis and the lift coefficient data. The slight asymmetry seen in data for symmetric cases is due to that the sampling is not sufficient large, slow oscillation occur with a period of  $\sim 20$  seconds. A clear correlation between entrainment and the envelope shape of the signal can be obtained by study how the corresponding DMD for entrainment correlates with the envelope (from the prestudy of regular, sampling over a whole entrainment period). This is also confirmed in a related study [17]. DMD is suitable to reconstruct flows and therefore more precisely estimate frequencies but it requires some caution, the DMD provides no physics, its a book keeping, inadequate sampling or choice of DMD in reconstruction of flow and the description of physics is altered.

Figure 14: DMD modes with most stationary character and highest energy, selected in accordance to Figure 12. From upper to lower: r, ta, tw and tt



## Conclusion

By disrupting the synchronization by using twisting and tapering for a bluff-body, the shear layers do not synchronize over the opposite side of the cantilever and hence gives a reduction of dynamical response in the force statistic on the cantilever surface. But, the force magnitude on the surface remains the same, i.e. a static force on average same magnitude as the dynamical RMS of the lift force. A PSD/FFT analysis at probe points on velocity components (PSD) respectively pressure (FFT) show how the layers are re-synchronized further downstream. DMD analysis shows for the three different designs of cantilevers no vorticity in the vicinity of the cantilever. The wake is elongated, but further downstream, the layers synchronize to form the vortex street and the oscillation pattern reflects the shape of the cantilever. The actual net gain by twisting/tapering remains unclear due to the entrainment is different and domain dependent.

## REFERENCES

- [1] J.A Amin and A.K. Ahuja, "Aerodynamic modification to the shape of the buildings: a review of the state-of-the-art", *Asian Journal of Civil engineering (Building and housing)* vol 11, no 4 (2010) pp. 433-450.
- [2] J.W. Tang, Y.M. Xie, P.Felicetti, J.Y. Tu, and J.D.Li, "Numerical simulations on straight and twisted polygonal buildings", *Struct. Design. Tall Spec.* Vol 22, 62-73 (2013).
- [3] J.H. Jung, and H.S. Yoon, "Large Eddy Simulation of flow past a twisted cylinder", *Proceedings of the 2013 International Conference on Mechanics, Fluids, Heat, Elasticity and Electromagnetic Fields*.
- [4] P.J. Schmid, "Dynamic mode decomposition of numerical and experimental data", *J. Fluid. Mech.* vol 656, pp 5-28 (2010).
- [5] S. Bagheri, "Koopman-mode decomposition of the cylinder wake", *J. Fluid Mech.* vol 726, pp 596-623 (2013).
- [6] OpenFoam, an open source CFD software package, <http://www.openfoam.org>.
- [7] H. Jasak, H.G Weller and A.D. Gosmani, "High resolution NVD differencing scheme for arbitrarily unstructured meshes", *International Journal for Numerical Methods in Fluids* Vol 31, pp. 431-449 (1999)
- [8] M. Germano, U. Piomelli, P. Moin, W.H. Cabot, "A Dynamic subgrid-scale eddy viscosity model", *Phys. Fluids A.* Vol 3, pp. 1760, (1991)
- [9] Ahmad Sohankar, L.Davidson and C.Norberg, "Large Eddy Simulation of Flow Past a Square Cylinder: Comparision of Different Subgrid Scale Models", *Journal of Fluids Engineering* Vol.122 , pp 39-47 (2000).
- [10] Fernando F. Grinstein and Christer Fureby, "On Flux-Limiting-Based Implicit Large Eddy Simulation", *J. Fluids Eng.* 129(12), 1483-1492 (Jul 19, 2007) (10 pages)
- [11] Christophe Geuzaine and Jean-François Remacle, "Gmsh: a three-dimensional finite element mesh generator with built-in pre- and post-processing facilities", *International Journal for Numerical Methods in Engineering*, 79(11), pp. 1309-1331 (2009).
- [12] J. Revstedt, "Interaction between an incompressible flow and elastic cantilevers of circular cross-section, *Int. J. Heat Fluid Flow*, Vol 43 pp 244- 250 (2013)
- [13] S. Dutta, P.K. Panigrahi, and K.Muralidhar, "Experimental Investigation of Flow Past a Square Cylinder at an Angle of Incidence", *Journal of Engineering Mechanics* vol 134 No 9, pp 788-803.
- [14] D.Sumner, "Flow above the free end of a surface-mounted finite-height circular cylinder: A review". *J. Fluid and Struct.* vol 43 , pp 41-63 (2013).
- [15] N. Rostamy, J.F. McClean, D. Sumner, DJ Begstrom, J.D. Bugg, "Flow above the free end of a surface-mounted square prism", *The Seventh International Colloquium on Bluff Body Aerodynamics and Applications (BBAA7) Shanghai, China, Sept 2-6 (2012)*.
- [16] Seyed Mohammad Hajimirzaie, "Flow structure in the wake of a low-aspect-ratio-wall-mounted bluff body", *University of Iowa (2013)*
- [17] A. Cesur, "On the Wake Structure of Flow Around Deforming and Vibrating Bodies", *PhD. Thesis, Lund University, Sweden (2013)*.